A new morphological segmentation algorithm for biomedical imaging applications

D. Gorpas[*a], P. Maragos[b], D. Yova[a]
[a] Laboratory of Biomedical Optics and Applied Biophysics, School of Electrical and Computer Engineering, National Technical University of Athens, GR-157 80, Zografou, Greece
[b] Computer Vision and Speech Laboratory, School of Electrical and Computer Engineering, National Technical University of Athens, GR-157 80, Zografou, Greece

ABSTRACT

Images of high geometrical complexity are found in various applications in the fields of image processing and computer vision. Medical imaging is such an application, where the processing of digitized images reveals vital information for the therapeutic or diagnostic algorithms. However, the segmentation of these images has been proved to be one of the most challenging topics in modern computer vision algorithms. The light interaction with tissues and the geometrical complexity with the tangent objects are among the most common reasons that many segmentation techniques nowadays are strictly related to specific applications and image acquisition protocols. In this paper a sophisticated segmentation algorithm is introduced that succeeds into overcoming the application dependent accuracy levels. This algorithm is based on morphological sequential filtering, combined with a watershed transformation. The results on various biomedical test images present increased accuracy, which is independent of the image acquisition protocol. This method can provide researchers with a valuable tool, which makes the classification or the follow-up faster, more accurate and objective.

Keywords: Morphological sequential filtering, watershed transformation, biomedical image segmentation, contrast enhancement, image gradient, regional minima.

1. INTRODUCTION

Biomedical imaging applications have become a valuably tool in modern healthcare, as they provide critical information for the diagnosis and the applied therapeutic process of various diseases. However, the processing of the acquired images is among the most challenging problems in computer vision field. Light interaction with tissue and the geometrical complexity of the inspected regions prevent from the development of sufficient algorithms that would lead to the extraction of accurate data. Despite the recent advantage of computer vision systems and methods, there is still lack of an algorithm that would successfully confront most of the biomedical imaging applications.

In literature, one can seek numerous methods for processing and segmenting medical images, many of them with quite accurate results[1]. Nevertheless, most of these methods fail when the acquisition protocol changes, or they are applied to a different application. The image processing and segmentation method, described in this paper, attempts to fulfill this lack of an algorithm that would semi-automatically adapt to the most common biomedical imaging applications.

The computer vision algorithm presented in this paper, for accurate image segmentation, is based on morphological sequential filtering[2, 3] and watershed transformation[2, 3, 4, 5]. Cascading erosions at multiple scales, alternating with image reconstructions, have been applied to produce image smoothing, progressively from the smallest scale up to the maximum. Through this procedure, contrast enhancement and significant de-noising is achieved[4]. The resulting edge weakening is overcoming with the application of Sobel filtering[3]. Finally, a marker controlled watershed transformation[2, 3, 4] is applied to segment the acquired images. This transformation utilizes an extended minima transformation, followed by a distance transformation[3, 6]. The segmentation is achieved by extracting the regional minima that occur only at the marked locations, and using these minima as flooding sources, the watershed transformation is applied[2]. Once the set of regions has been identified, the properties of these regions become the input to following procedures that perform decision-making tasks, such as recognition or inspection.

[*] dgorpas@mail.ntua.gr; phone +302107722293; fax +302107723894

Image Processing: Machine Vision Applications II, edited by Kurt S. Niel, David Fofi, Proc. of SPIE-IS&T Electronic Imaging, SPIE Vol. 7251, 72510C · © 2009 SPIE-IS&T · CCC code: 0277-786X/09/$18 · doi: 10.1117/12.805574

The proposed algorithm has been tested over two medical imaging applications. The first one is the optical imaging of skin lesions, where image segmentation is important for the follow-up of the therapeutic process or the diagnosis. Although these categories of images usually contain one object, the accurate segmentation is a difficult process, due to strong tissue scattering. The proposed algorithm successfully overcame this problem presenting 95% accurate segmentation, compared to detailed manual segmentation.

The second application is the processing in light microscopy imaging. Modern diagnostic algorithms are strictly related to the cell geometry, texture and/or color characteristics. Nevertheless, the most challenging aspect is the successful segmentation of the cells. The geometry complexity here is very high, with strong background in-homogeneity. However, the proposed algorithm preliminary presented 80% successful cell segmentation, even in cases of tangent cells.

This paper is organized as follows: In Section 2 the methodology of the proposed algorithm is presented. The image preprocessing and segmentation are briefly described and their main points are highlighted. In Section 3 the two biomedical imaging applications and the image acquisition are presented. Finally, in Section 4 the results of the proposed algorithm on the two imaging applications are given, while the paper concludes with a brief discussion in Section 5.

2. METHODOLOGY

Image segmentation is among the most challenging problems in the field of computer vision. Generally speaking, segmentation is the process of isolating objects in the image from the background, i.e partitioning the image into disjoint regions, each one being homogeneous and connected with respect to some property, such as gray value or texture[7]. In this section the proposed algorithm is presented, divided into two different stages: (a) preprocessing and image simplification and (b) the region based watershed transformation that leads to the segmentation of the image.

All the algorithms presented in this section are referred to gray-scale images. The transformation from RGB images to gray-scale has been succeeded by selection of the green channel of the RGB images, since this is the channel bearing the more information, according to the CCD camera structure.

2.1 Image simplification

The image preprocessing and simplification, in the context of image segmentation, is of critical importance since its output determines directly the segmentation results. The main objective of this stage is to reduce the presence of noise, producing an image that consists mostly of flat and large regions. There have advance to the pre-processing algorithms over the years, however a large number of them yet requires at some point thresholding, an action that makes the algorithm problem-dependent.

Biomedical images suffer from inhomogeneous background, with very low contrast, complex structure and often overlapping components. This fact makes the application of any kind of thresholding at the stage of preprocessing an uncertain action, as it may influence negatively the outcomes of the segmentation and make the algorithm applicable only to a specific type of biomedical images and acquisition protocol. In order to avoid this drawback the proposed algorithm has adopted a morphological sequential filtering process, known as alternating sequential filtering[2, 8, 9] (ASF), and obtained by applying sequential erosions followed by image reconstructions.

However prior to the ASF, intensity adjustment is applied. The scope of this process is to expand the histogram of all input images to the same histogram boundaries. The intensity adjustment, commonly known as contrast-stretching operator, is a point operator that uses a piecewise smooth function of the input gray level to enhance important details of the image[3]. Because the described algorithm has been developed for various acquisition protocols, this smoothing function is a linear one, targeting not to the enhancement but to the distribution of the intensity levels between black (0) and while (1).

Now that all the input images are expanded between the same histogram boundaries, the morphological filtering is applied. The most common formalism of the ASF family is the one involving cascading open-closings $b_t a_t$ at multiple scales $t = 1,\ldots,r$, where $a_t\left(f\right) = f \circ tB$ is the opening transformation of the image input f with the structuring element B at the scale t and $b_t\left(f\right) = f \bullet tB$ is the closing transformation[8, 9]. This generates a class of efficient nonlinear smoothing filters

$$\psi_{asf}(f) = b_r a_r \left(\cdots \left(b_2 a_2 \left(b_1 a_1 (f) \right) \right) \right) \tag{1}$$

with the smoothing progressively increases from the smallest scale possible up to a maximum scale r.

In this paper, the approach of equation (1) will be retained. Nevertheless, instead of sequential openings and closings, cascading erosions followed by reconstruction are applied. The reconstruction scheme that has been used is the morphological reconstruction by dilation[2, 4] of a gray-scale mask image, g, by a gray-scale marker image, f, defined as the geodesic dilation of f with respect to g, iterated until stability is reached. The geodesic dilation[3, 10] of f with respect to g is defined as:

$$D_g^{(1)}(f) = (f \oplus B) \wedge g \tag{2}$$

where $\wedge$ denotes the point-wise minimum operator[4]. Equation (2) indicates that the geodesic dilation of size 1 is obtained by firstly computing the dilation of f by the structuring element B and then selecting the minimum between the result and the mask image g at every pixel point (u, v) of the image plane. With respect to (2) the geodesic dilation of size t of input image f with respect to g is defined as:

$$D_g^{(t)}(f) = D_g^{(1)}\left[D_g^{(t-1)}(f) \right] \tag{3}$$

with $D_g^{(0)}(f) = f$.

With equation (3) as a premise, the morphological reconstruction by dilation is expressed by the formalism:

$$R_g^D(f) = D_g^{(k)}(f) \tag{4}$$

with k being the scale that leads to:

$$D_g^{(k)}(f) = D_g^{(k+1)}(f) \tag{5}$$

Thus, the operator that is applied to the image, after the contrast-stretching process, is described by:

$$O_R^{(t)}(f) = R_f^D(f \ominus tB) \tag{6}$$

which is the reconstruction by dilation of f from the erosion of size t of f, process knowing and as opening by reconstruction. The operator of equation (6) is applied sequentially to the gray-scale image f and to its complement, treating symmetrically the image foreground and background and thus accomplishing image simplification and denoising, without affecting the position of the boundaries of the regions of interest.

One question, that may arise at this point, is the determination of the iterations number. By applying the algorithm to various test images, it has been observed that using more than six scales does not change the segmentation outcomes at the objects of interest. As a result the described algorithm has been set to six iterations of the alternating sequential filter, giving, as an extension, the opportunity to the user to try less or more scales if he desires to.

However, the boundaries strength of these regions has been affected by the application of the sequential morphological filter. This fact leads either to the expansion or to the reduction of the segmented area. Among the numerous edge strengthening filters, the Sobel filter[2, 3, 11, 12] has been proven to provide rapid and sufficient results and thus it is the one selected for the described algorithm. This high-pass filter operator utilizes the following 3×3 masks (Sobel masks):

$$\begin{bmatrix} -1 & -2 & -1 \\ 0 & 0 & 0 \\ 1 & 2 & 1 \end{bmatrix} \quad \text{and} \quad \begin{bmatrix} -1 & 0 & 1 \\ -2 & 0 & 2 \\ -1 & 0 & 1 \end{bmatrix}$$

These two masks are convolved with the image separately, to measure the strength of horizontal and vertical edges, respectively, present at each pixel. Thus, the gradient magnitude image of the sequential morphological filtering output is computed by approximating the first derivatives G_u and G_v at each pixel. The two strengths are then combined to find the total amount to which any edge exists at the pixel (u, v), that is:

$$G_{uv} = \left[G_u^2 + G_v^2 \right]^{1/2} \tag{7}$$

2.2 Image segmentation

As it has been already mentioned, the segmentation process in the described algorithm for biomedical images is based on the well-known watershed transformation. However, direct application of the watershed transformation to the gradient image of equation (7) would lead to over-segmentation due to local irregularities of the gradient. A practical solution to this problem is to limit the number of allowable regions by incorporating a preprocessing stage, designed to bring additional knowledge into the segmentation procedure. Hence, instead of the simple watershed transformation, a marker-controlled watershed based segmentation[2, 4, 13 – 15] has been adopted.

A marker is a connected component belonging to an image. The segmentation process starts with creating flooding waves that emanate from the set of markers and flood the image gradient surface. The points where the emanating waves meet each other form the segmentation boundaries[2, 3]. The simplest markers are the regional minima of the gradient image, but very often they are extremely numerous and lead to over-segmentation[2]. One approach to control this over-segmentation is based on the concept of internal and external markers. The internal markers are localized inside each of the objects of interest, while the set of external markers is contained within the background.

In order to identify the internal markers, the extended minima transformation has been applied to the gradient image. The regional minima transform identifies connected components of pixels with a constant intensity value, and whose external boundary pixels all have a higher value. However, most of the regional minima specified are very swallow and represent detail that is irrelevant to the segmentation problem. For these extraneous minima to be eliminated, a threshold height is included to the regional minima transformation. This threshold determines whether a set of connected pixels belong to the foreground or the background of the gradient image and its value is assigned according to the type of objects of interest. Thus for each application a unique threshold height has been assigned, permitting, as well, the user to modify this value if the results are not satisfying.

The next step is to identify the external markers, or pixels that belong to the background. The approach that has been adopted is to mark the background by finding pixels that are exactly midway between the internal markers. This is implemented by computing the watershed transformation of the Euclidian distance transform[10, 16, 17] of the internal marker image.

Given both internal and external markers, the gradient image is modified so that regional minima occur only in the marked locations, while other pixel values are "pushed up" as necessary to remove all other regional minima. The resulted gray-level image is the one that finally undergoes a watershed transformation, action that concludes the proposed algorithm for segmenting biomedical images.

3. DATA

The proposed algorithm has been tested at two different types of medical imaging applications. The first one is the optical imaging of skin lesions, and more specific from SKH-HR1 albino hairless mice, bearing non-melanoma skin carcinomas (NMSC). The images were acquired after the application of photodynamic therapy for evaluation purposes. The geometrical features of the presented tumours are of great importance for the therapy monitoring. Since the imaging system is un-calibrated, a calibration sphere is also present to assist for the quantification of the geometrical features of the tumours. In Fig. 1 are shown the RGB and gray-level images of such an acquisition.

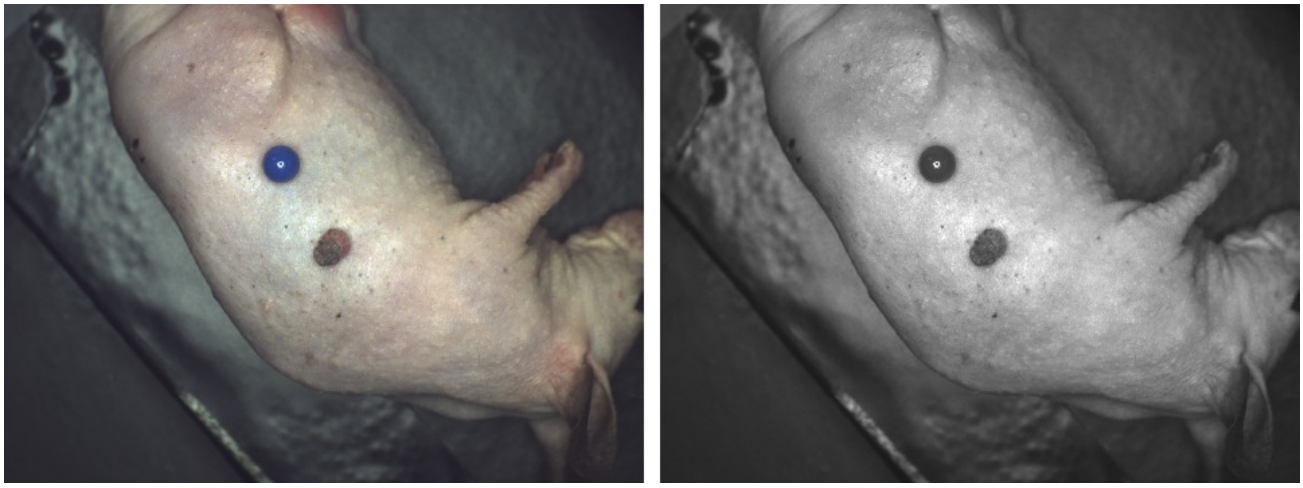

Fig. 1: A non-melanoma skin carcinomas animal model as acquired from an optical imaging system (left) with a calibration sphere on the model surface and the green channel (right) of the RGB image.

The second application that was used to evaluate the proposed algorithm is light microscopy imaging. Images of prostate cancer nuclei were acquired using a light microscope and a thermoelectrically cooled color CCD camera. Features related to the nuclei, such as color and intensity metrics, are often used to determine the cell nucleus DNA index, and thus the extraction of the nuclei from the image background is of great importance. In Fig. 2 the acquired RGB image of prostate cancer nuclei is presented, along with the corresponding gray-level image.

The animal model treatment and all the measurements involved in this paper were carried out according to the strict guidelines, established by the European Council Directive 86/909/EC and the Greek Committee for animal models.

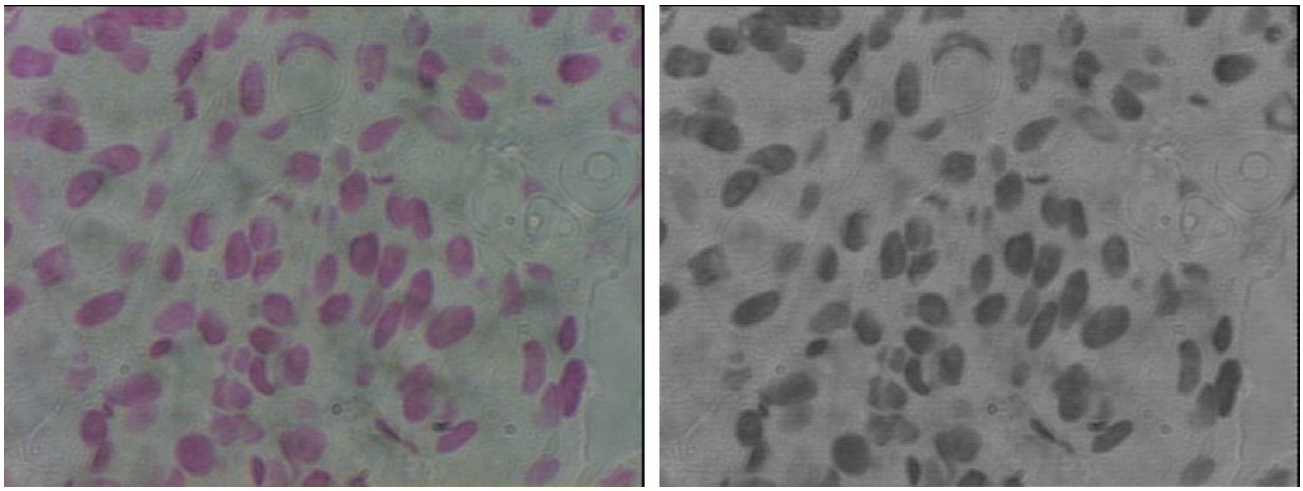

Fig. 2: Prostate cancer nuclei as acquired using a light microscope (left) and its green channel (right).

4. RESULTS

The results presented in this section are grouped between the above-mentioned cases. The entire segmentation process for both cases was implemented fully automatic. The only requirement was the user to define the type of application image, so the corresponding threshold height to be considered.

4.1 Optical imaging

The segmentation application of Fig. 1, although it seems to be quite simple, is among the most difficult applications as it includes light interaction with tissue, a highly scattering media. The reflectance levels just around the two objects of interest lead most of the common segmentation algorithms to fail and a preprocessing of the acquired images is essential.

In Fig. 3 is presented the gray-level image after it has been undergo by the contrast-stretching process with respect to the green channel of the original image. It becomes apparent that through the linear intensity adjustment, a significant improvement is succeeded.

Fig. 3: The green channel of the acquired image (left) and the improved image after the intensity adjustment (right).

In order to simplify the image of Fig. 3 the sequential morphological filter is applied. The results of this filter at the six scales are presented in Fig. 4.

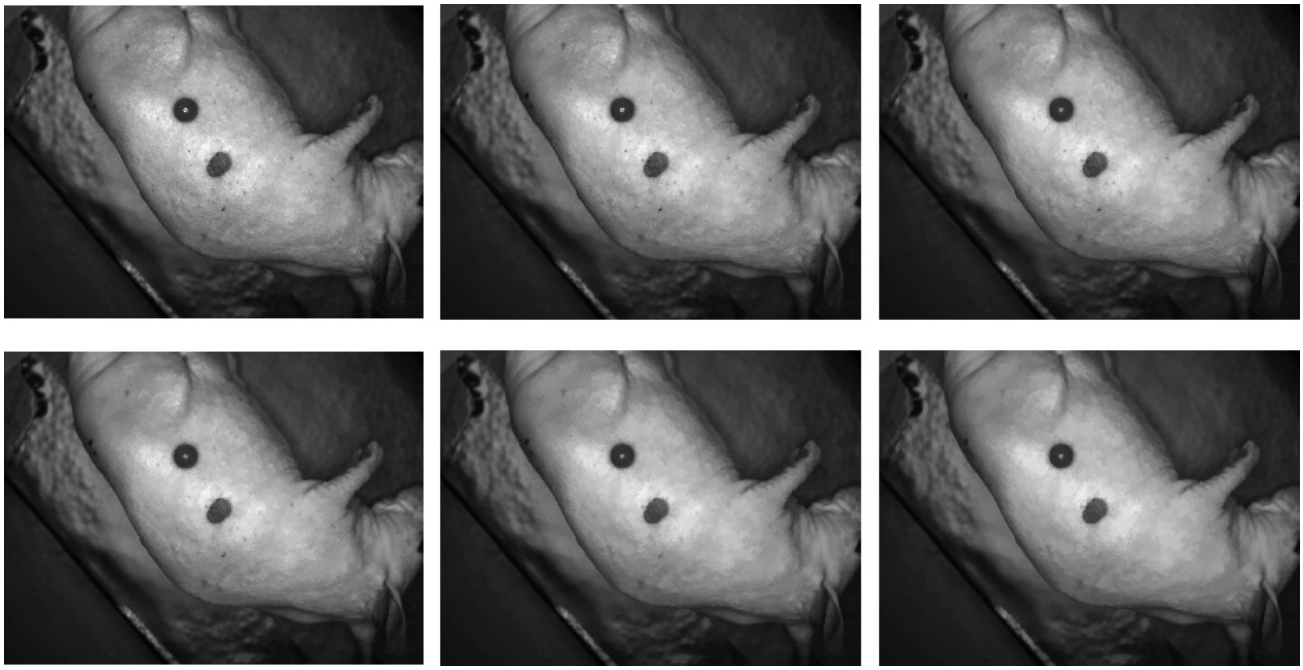

Fig. 4: Results of the alternating sequential filter at the applied six levels (the first three shown at the top row and the latter three at the second row moving from left to right). The smoothing that is achieved is apparent at these images. Further filtering will produce no better results at the segmentation algorithm.

Finally in Fig. 5 are shown the gradient image derived after the Sobel filtering, the internal and external marker set, the gradient image after the modification of the gradient image and the final segmented image.

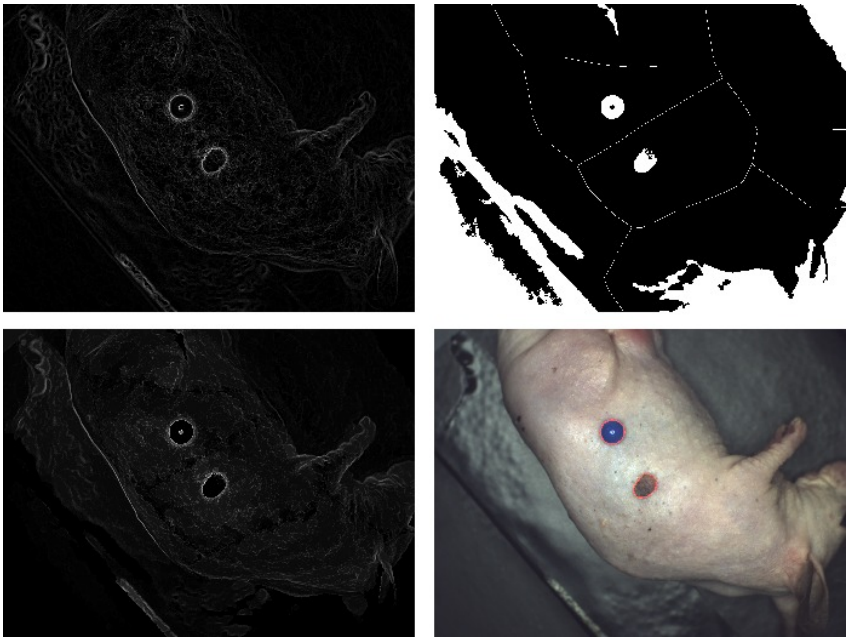

Fig. 5: The gradient output image of the Sobel Filter (top left), the external and internal markers (top right), the modified gradient image (bottom left) and the segmented image (bottom right) after boundary objects have been removed.

From Fig. 5 becomes apparent that the application of the watershed transformation to the modified gradient image provides very accurate segmentation results, suitable for tissue lesion monitoring applications. The described algorithm has been tested over various images of the same medical application and the results were compared to the most accurate but time-consuming manual segmentation. The comparison revealed a mean 95% accuracy over the results of the proposed algorithm at various geometrical features, such as area and axis lengths. Furthermore, in some cases there was the need for the user to interact with the algorithms outcomes, in order to isolate the objects of interest for some unwanted image segments.

4.2 Light microscopy imaging

With a similar modus operandi as in the previous case, various images of the light microscopy imaging application were tested with the described algorithm. In Fig. 6 are shown the green channel of the acquired image and the adjusted for the intensity gray-scale image.

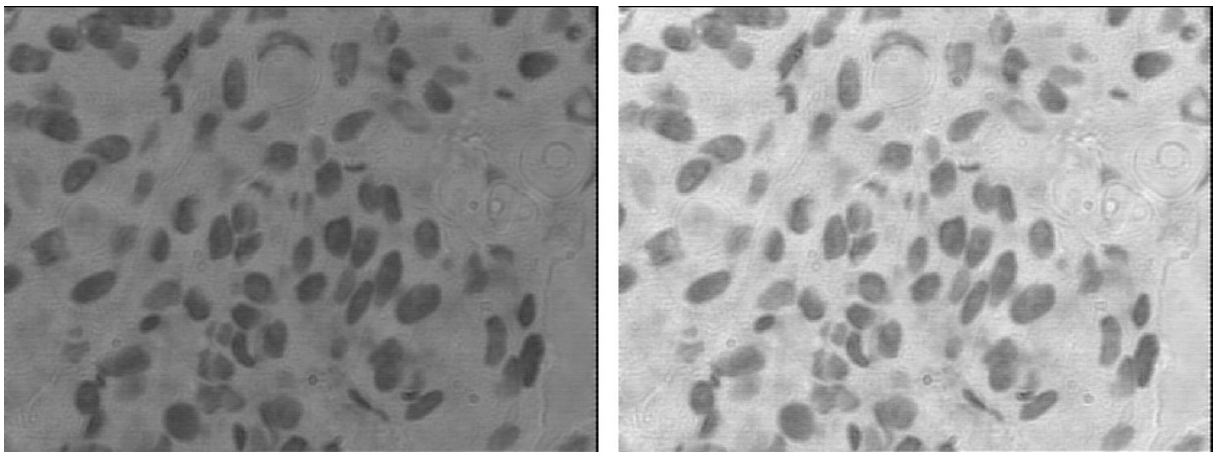

Fig. 6: The green channel of the acquired image (left) and the improved image after the intensity adjustment (right).

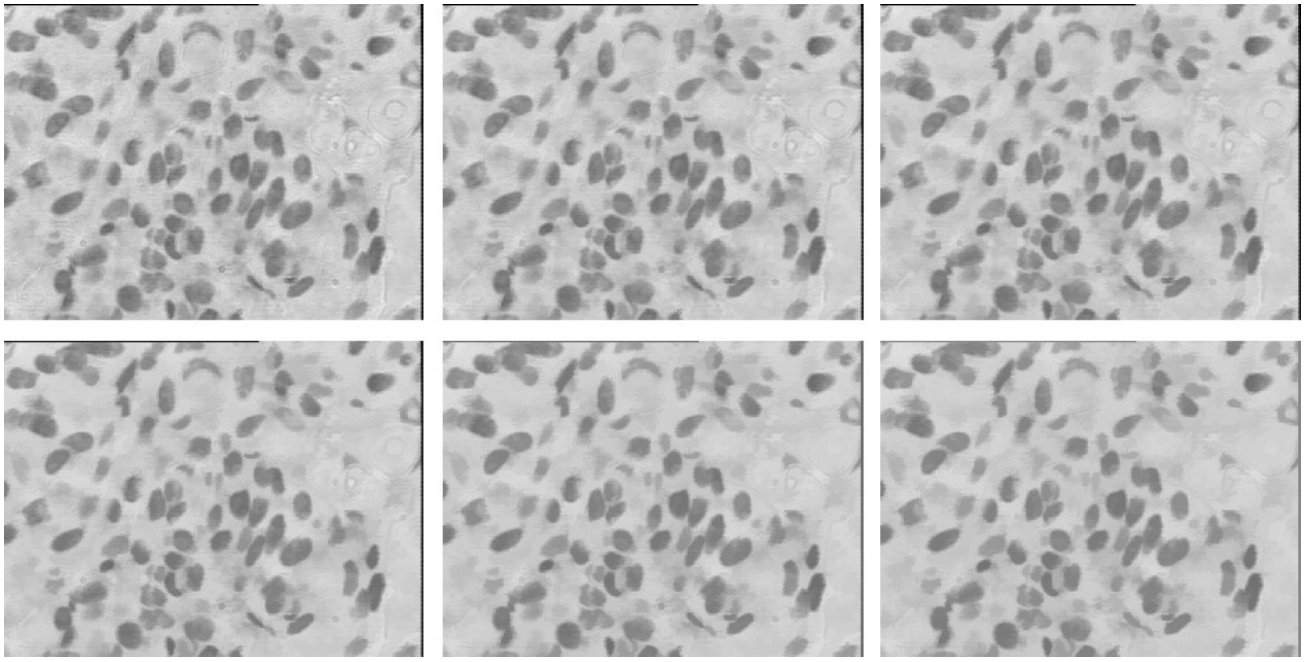

Fig 7: Results of the alternating sequential filter at the applied six levels (the first three shown at the top row and the latter three at the second row moving from left to right). The background smoothing is obvious.

Furthermore, the alternating morphological filter results on this type of application are presented in Fig. 7. From this figure one can notice how the background is improved between the different scales of the filter and the initial gray-level image. This smoothing is of great importance for the segmentation process. The gradient image, the markers, the modified gradient image and finally the segmentation results are all shown in Fig. 8. Due to the inconsistency of the background and of some of the cells nuclei, there has been some unwanted regions included and some boundary shrinkage to some of the nuclei. The unwanted regions can very easily be rejected with a color or shape algorithm, topic that belongs to a decision-making algorithm (besides the background regions, some cell nuclei must also be rejected as they are positioned to a deeper lever than the surface). Having trying the algorithm to various images of the same application, a successful recognition of cell nuclei up to 80% has been succeed, in comparison to the manual count.

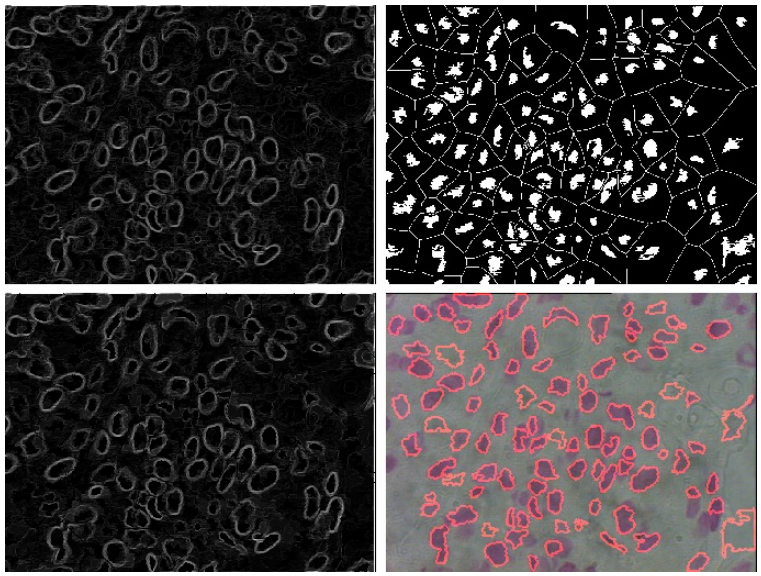

Fig. 8: The gradient output image of the Sobel Filter (top left), the external and internal markers (top right), the modified gradient image (bottom left) and the segmented image (bottom right) after boundary objects have been removed.

5. DISCUSSION

Future work with this algorithm is to define a fully automated threshold height assignment, related to specific image features. As this threshold is not a grey-level value for transformation into binary image, many of the well-known threshold algorithms, like Otsu's method[3], fail to provide a value that would lead to accurate segmentation. However, more medical imaging applications should be tested, before a method of the threshold value to be developed.

As a segmentation algorithm, this method does not include a process for determining which of the recognized objects are worth keeping and which are not. Furthermore, there is need for visually well-defined objects to exist; otherwise it will fail to produce accurate results. Finally, as this algorithm perform object labeling after the segmentation, in order to correctly label the segmented object the input images should be in the fashion of the background bearing higher intensity values than the foreground, otherwise the background would be labeled, instead of the segmented objects.

A robust segmentation algorithm, which manages to overcome the application-related accuracy that dominates the most state-of-the-art segmentation procedures in the biomedical image processing, was developed. The results presented high accuracy levels in two different imaging applications. This method can provide researchers with a valuable tool, which makes the classification or the follow-up faster and more accurate.

REFERENCES

[1] Zhu L., Qin S., Zhou F., "*Skin image segmentation based on energy transformation*", J. Biomed. Opt. **9**, 362-366 (2004).

[2] Gonzalez R.C., Richard E.W., "Digital image processing", Pearson Prentice Hall, Third Edition, USA (2008).

[3] Bovik A., "Handbook of Image and Video Processing", Elsevier Academic Press, Second Edition, USA (2005).

[4] Sofou A., Tzafestas C., Maragos P., "*Segmentation of Soilection Images Using Connected Operators*", Proc. Int. Conf. Image Processing, Greece, 1087-1090 (2001).

[5] Beucher S., "*The watershed transformation applied to image segmentation*", Scan. Microsc. Int. **6**, 299–314 (1992).

[6] Shapiro L.G., Stockman G.C., "*Computer Vision*", Prentice-Hall Inc., USA (2001).

[7] Sofou A., Evangelopoulos G., Maragos P., "*Soil Image Segmentation and Texture Analysis: A computer Vision Approach*", IEEE Geosci. Remote Sens. **2**, 394-398 (2005).

[8] Couprie M., Bertrand G., "*Topology preserving alternating sequential filter for smoothing two-dimensional and three-dimensional objects*", J. Electron. Imaging **13**, 720-730 (2004).

[9] Dougherty E.R., "*Automatic design of morphological operators*", J. Electron. Imaging **13**, 486-491 (2004).

[10] Pastore J.I., Moler E.G., Ballarin V.L., "*Segmentation of brain magnetic resonance images through morphological operators and geodesic distance*", Digit. Signal Process. **15**, 153-160 (2005).

[11] Davies E.R., "*Machine vision: Theory, Algorithms, Practicalities*", Elsevier Inc., Third Edition, USA (2005).

[12] Kotera H., Wang H., "*Multiscale image sharpening adaptive to edge profile*", J. Electron. Imaging **14**, 013002 (2005).

[13] Beucher G., Meyer F., "The Morphological approach of segmentation: the watershed transformation", in Dougherty E. editor, Mathematical Morphology in Image Processing, Marcel Dekker, New York, (1992).

[14] Hu Y., Nagao T., "A matching method based on marker-controlled watershed segmentation", in Proc. IEEE International Conference on Image Processing, 283-286 (2004).

[15] Yan J., Zhao B., Wang L., Zelenetz A., Schwartz L.H., "*Marker-controlled watershed for lymphoma segmentation in sequential CT images*", Med. Phys. **33**, 2452-2460 (2006).

[16] Huang C.T., Mitchell O.R., "*An Euclidean Distance Transform Using Grayscale Morphology Decomposition*", IEEE Trans. Pattern. Anal. Mach. Intell. **16**, 443-448 (1994).

[17] Byoung-Ki Jeon B.K., Jang J.H., Hong K.S., "*Robust region segmentation based on a pseudo-distance map*" J. Electron. Imaging **13**, 602-612 (2004).